

Optimally chirped multimodal CARS microscopy based on a single Ti:sapphire oscillator

Adrian F. Pegoraro^{1,2}, Andrew Ridsdale², Douglas J. Moffatt², Yiwei Jia³ John Paul Pezacki², and Albert Stolow^{1,2,*}

¹ Department of Physics, Queen's University, Kingston, Ontario, K7L 3N6 Canada

² Steacie Institute for Molecular Sciences, National Research Council of Canada, Ottawa, Ontario, K1A 0R6 Canada

³ Scientific Equipment Group, Olympus America Inc., 3500 Corporate Parkway, P.O. Box 610, Central Valley, PA, 18034, USA

*Corresponding Author: A. Stolow

albert.stolow@nrc-cnrc.gc.ca

Abstract: We demonstrate high performance coherent anti-Stokes Raman scattering (CARS) microscopy of live cells and tissues with user-variable spectral resolution and broad Raman tunability (2500 - 4100 cm⁻¹), using a femtosecond Ti:Sapphire pump and photonic crystal fiber output for the broadband synchronized Stokes pulse. Spectral chirp of the fs laser pulses was a user-variable parameter for optimization in a spectral focussing implementation of multimodal CARS microscopy. High signal-to-noise, high contrast multimodal imaging of live cells and tissues was achieved with pixel dwell times of 2-8 μ s and low laser powers (< 30 mW total).

© 2009 Optical Society of America

OCIS codes: (170.5810) Scanning microscopy; (180.4315) nonlinear microscopy (300.6230) Spectroscopy; coherent anti-Stokes Raman scattering.

References and links

1. A. Zumbusch, G. R. Holtom, and X. S. Xie, "Three-Dimensional Vibrational Imaging by Coherent Anti-Stokes Raman Scattering," *Phys. Rev. Lett.* **82**, 4142–4145 (1999).
2. J.-X. Cheng and X. Xie, "Coherent Anti-Stokes Raman Scattering Microscopy: Instrumentation, Theory, and Applications," *J. Phys. Chem. B* **108**, 827–840 (2004). URL http://pubs3.acs.org/acs/journals/doi/lookup?in_doi=10.1021/jp035693v.
3. W. Denk, J. Strickler, and W. Webb, "Two-photon laser scanning fluorescence microscopy," *Science* **248**, 73–76 (1990).
4. P. J. Campagnola, M.-d. Wei, A. Lewis, and L. M. Loew, "High-Resolution Nonlinear Optical Imaging of Live Cells by Second Harmonic Generation," *Biophys. J.* **77**, 3341–3349 (1999).
5. D. Yelin and Y. Silberberg, "Laser scanning third-harmonic-generation microscopy in biology," *Opt. Express* **5**, 169–175 (1999). URL <http://www.opticsexpress.org/abstract.cfm?URI=oe-5-8-169>.
6. X. Nan, A. M. Tonary, A. Stolow, X. S. Xie, and J. P. Pezacki, "Intracellular Imaging of HCV RNA and Cellular Lipids by Using Simultaneous Two-Photon Fluorescence and Coherent Anti-Stokes Raman Scattering Microscopies," *ChemBioChem* **7**, 1895–1897 (2006).
7. T. T. Le, I. M. Langohr, M. J. Locker, M. Sturek, and J.-X. Cheng, "Label-free molecular imaging of atherosclerotic lesions using multimodal nonlinear optical microscopy," *J. Biomed. Opt.* **12**, 054007 (pages 10) (2007). URL <http://link.aip.org/link/?JBO/12/054007/1>.

8. D. J. Jones, E. O. Potma, J. xin Cheng, B. Burfeindt, Y. Pang, J. Ye, and X. S. Xie, "Synchronization of two passively mode-locked, picosecond lasers within 20 fs for coherent anti-Stokes Raman scattering microscopy," *Rev. Sci. Instrum.* **73**, 2843–2848 (2002). URL <http://link.aip.org/link/?RSI/73/2843/1>.
9. F. Ganikhanov, S. Carrasco, X. S. Xie, M. Katz, W. Seitz, and D. Kopf, "Broadly tunable dual-wavelength light source for coherent anti-Stokes Raman scattering microscopy," *Opt. Lett.* **31**, 1292–1294 (2006). URL <http://ol.osa.org/abstract.cfm?URI=ol-31-9-1292>.
10. C. Heinrich, A. Hofer, A. Ritsch, C. Ciardi, S. Bernet, and M. Ritsch-Marte, "Selective imaging of saturated and unsaturated lipids by wide-field CARS-microscopy," *Opt. Express* **16**, 2699–2708 (2008). URL <http://www.opticsexpress.org/abstract.cfm?URI=oe-16-4-2699>.
11. J.-x. Cheng, A. Volkmer, L. Book, and X. Xie, "An Epi-Detected Coherent Anti-Stokes Raman Scattering (E-CARS) Microscope with High Spectral Resolution and High Sensitivity," *J. Phys. Chem. B* **105**, 1277–1280 (2001). URL <http://pubs3.acs.org/acs/journals/doi/lookup?in.doi=10.1021/jp003774a>.
12. N. Dudovich, D. Oron, and Y. Silberberg, "Single-pulse coherently controlled nonlinear Raman spectroscopy and microscopy," *Nature* **418**, 512–514 (2002).
13. E. T. J. Nibbering, D. A. Wiersma, and K. Duppen, "Ultrafast nonlinear spectroscopy with chirped optical pulses," *Phys. Rev. Lett.* **68**, 514–517 (1992).
14. A. M. Zheltikov and A. N. Naumov, "High-resolution four-photon spectroscopy with chirped pulses," *Quantum Electron.* **30**, 606–610 (2000). URL <http://stacks.iop.org/1063-7818/30/606>.
15. T. Hellner, A. M. Enejder, and A. Zumbusch, "Spectral focusing: High spectral resolution spectroscopy with broad-bandwidth laser pulses," *Appl. Phys. Lett.* **85**, 25–27 (2004). URL <http://link.aip.org/link/?APL/85/25/1>.
16. I. Rocha-Mendoza, W. Langbein, and P. Borri, "Coherent anti-Stokes Raman microspectroscopy using spectral focusing with glass dispersion," *Appl. Phys. Lett.* **93**, 201103 (pages 3) (2008). URL <http://link.aip.org/link/?APL/93/201103/1>.
17. R. M. Onorato, N. Muraki, K. P. Knutsen, and R. J. Saykally, "Chirped coherent anti-Stokes Raman scattering as a high-spectral- and spatial-resolution microscopy," *Opt. Lett.* **32**, 2858–2860 (2007). URL <http://ol.osa.org/abstract.cfm?URI=ol-32-19-2858>.
18. H. Lotem, R. T. Lynch, and N. Bloembergen, "Interference between Raman resonances in four-wave difference mixing," *Phys. Rev. A* **14**, 1748–1755 (1976).
19. K. M. Hilligsøe, T. Andersen, H. Paulsen, C. Nielsen, K. Mølmer, S. Keiding, R. Kristiansen, K. Hansen, and J. Larsen, "Supercontinuum generation in a photonic crystal fiber with two zero dispersion wavelengths," *Opt. Express* **12**, 1045–1054 (2004). URL <http://www.opticsexpress.org/abstract.cfm?URI=oe-12-6-1045>.
20. M. Shiomi, T. Ito, S. Yamada, S. Kawashima, and J. Fan, "Development of an Animal Model for Spontaneous Myocardial Infarction (WHHLMI Rabbit)," *Arterioscler Thromb Vasc Biol* **23**, 1239–1244 (2003).
21. *Raman/Infrared Atlas of Organic Compounds* (Verlag Chemie, Weinheim, 1978).
22. A. M.-A. Martin Schwartz and W. H. Koehler, "Fermi resonance in aqueous methanol," *J. Mol. Struct.* **63**, 279–285 (1980).
23. H. C. Strydom, A. B. Chandler, R. E. Dinsmore, V. Fuster, S. Glagov, J. Insull, William, M. E. Rosenfeld, C. J. Schwartz, W. D. Wagner, and R. W. Wissler, "A Definition of Advanced Types of Atherosclerotic Lesions and a Histological Classification of Atherosclerosis : A Report from the Committee on Vascular Lesions of the Council on Arteriosclerosis, American Heart Association," *Arterioscler Thromb Vasc Biol* **15**, 1512–1531 (1995). URL <http://atvb.ahajournals.org/cgi/content/abstract/15/9/1512>.
24. S. Murugkar, C. Brideau, A. Ridsdale, M. Naji, P. K. Stys, and H. Anis, "Coherent anti-Stokes Raman scattering microscopy using photonic crystal fiber with two closely lying zero dispersion wavelengths," *Opt. Express* **15**, 14,028–14,037 (2007). URL <http://www.opticsexpress.org/abstract.cfm?URI=oe-15-21-14028>.

1. Introduction

Coherent anti-Stokes Raman scattering (CARS) microscopy is a powerful imaging modality that continues to grow in significance due to its ability to provide label-free yet molecule-specific images of live cells and tissues [1, 2]. CARS microscopy is readily combined with other nonlinear imaging methods such as two-photon fluorescence (TPF) [3], second harmonic generation (SHG) [4], and third harmonic generation (THG) [5], generating a multimodal CARS microscopy [6, 7]. A key feature of CARS microscopy is its ability to tune through Raman resonances, providing the molecule-specific dimension of vibrational spectroscopy and all its attendant benefits. This spectral advantage applies especially to live cells and tissue where the heterogeneous nature of the sample can make identification of components more difficult if using nonresonant signals alone. To date, most implementations of CARS microscopy are based on the use of a pair of transform-limited (TL) tuneable picosecond (ps) pulses, obtained either

from electronically synchronized ps oscillators [8] or ps synchronously-pumped optical parametric oscillators (OPO) [9]. Some work has also been done using nanosecond lasers [10]. The high spectral resolution ($\sim 5 \text{ cm}^{-1}$) of these approaches permit microspectroscopic studies of spectral line shapes. The narrow linewidth of TL ps pulses ensures that the laser pulse linewidth falls within or matches the linewidth of the Raman band of interest, thereby enhancing the contrast of resonant over nonresonant (background) CARS signals [11]. This is especially important in the fingerprint region where the Raman bands can be narrow. CARS microscopy with ps laser pulses is equally successful at imaging the distributions of lipids and water within cells and tissues, even though the effective linewidths of these Raman bands are much greater (lipids $\sim 100 \text{ cm}^{-1}$, water $\sim 400 \text{ cm}^{-1}$) than the 5 cm^{-1} TL resolution of ps laser pulses. Interestingly, this raises the question as to whether broader bandwidth femtosecond (fs) pulses might also be well suited to the CARS imaging of lipids or water. Furthermore, in multimodal CARS microscopy, the nonresonant TPF, SHG and THG signals clearly benefit from the use of shorter (fs) laser pulses. Therefore, depending on the nature of the problem, it may be useful to reconsider the use of fs laser pulses in CARS microscopy. This immediately raises the concern of the poor spectral resolution inherent to TL fs pulses. In nonlinear optics, however, there exist alternate methods for enhancing spectral resolution in CARS microscopy based upon the high degree of control over optical phase that is implicit in fs laser pulses ([12]). By far the simplest such optical phase control is that of a quadratic spectral phase variation; in other words, a linear variation of the frequencies within the pulse, called chirp. By controlling the degree of chirp, high spectral resolution can be obtained in nonlinear spectroscopy when using broad-band fs laser pulses [13, 14]. In CARS microscopy, this method is called spectral focussing and was shown [15] to achieve Raman spectral resolution quite comparable ($\sim 8 \text{ cm}^{-1}$) to that achieved with TL ps pulses. This method supports both spectral tuning and high contrast imaging, however, due to the use of an amplified laser system, neither rapid imaging nor broad spectral tuning are easily achievable. A different implementation of this technique was also recently demonstrated [16]. The use of chirped pump pulses combined with dispersed detection has also been demonstrated in multiplex CARS microscopy [17].

Here we use the degree of linear chirp as a variable parameter to be optimized under user control so as to enhance both signals and contrast in high performance multimodal CARS microscopy. We show that the best performance (combination of signal and contrast) is obtained, as intuitively expected, when the effective laser linewidth at second order (i.e. the Raman resonance) matches the width of the Raman resonance under consideration. As Raman linewidths can vary considerably (e.g. $\sim 5\text{-}400 \text{ cm}^{-1}$) with molecular species, the ability to easily tune the effective spectral width of the excitation pulses should be a useful tool to put in the hands of the user. Furthermore, in multimodal imaging, TPF, SHG and THG all benefit as the intensity of the excitation pulses increases (i.e. as pulse durations decrease). By placing the effective Raman spectral width under user control, it offers a choice between higher spectral resolution in CARS versus intensity in these other channels, allowing the user to achieve optimal performance imaging for a particular sample. In our implementation, we desired broad Raman tunability ($\sim 2500\text{-}4100 \text{ cm}^{-1}$) and therefore used a photonic crystal fiber (PCF) to generate the broadband synchronized Stokes light. Rapid tuning of the Raman resonance is simply obtained by varying the time delay between chirped pump and Stokes pulses, whereas the effective Raman resolution and signal level are controlled by varying the chirp of the two pulses. The approach we describe is general to all fs sources and can also be used, for example, with synchronized fs oscillators or a fs OPO. Overall, the optimally chirped system is a high performance, versatile multimodal CARS microscope allowing for microspectral imaging of live cells and tissues. We provide sample illustrations of this capability by imaging myelin in rat dorsal nerves, an atherosclerotic arterial sample (rabbit aorta), and by monitoring lipid traf-

ficking in live human hepatocytes (liver cells). In the following, we first discuss from a theory point of view the motivation for the optimally chirped spectral focussing approach and suggest some operating parameters. We then describe the technical implementation and performance calibration of our multimodal CARS microscope. Finally, we apply this system to imaging in cells and tissues and provide representative images and video.

2. Theory

Prior modeling of CARS microscopy, based on measurements of polystyrene beads, showed that high contrast of resonant over nonresonant CARS signals requires a narrow (ps pulse) spectral width [11]. In the following, we consider more generally the implications of the pulse duration (spectral resolution) for a broad range of Raman bandshapes, anticipating that broader Raman linewidths (e.g. lipid, water) will benefit from the use of shorter (e.g. fs) pulses. Following reference [11], we calculate the CARS polarization. In order to make direct comparisons, we used the same parameters: a Raman shift of 1601 cm^{-1} with a pump center frequency of 13330 cm^{-1} and a Stokes center frequency of 11731 cm^{-1} . Using a Raman linewidth of 9.2 cm^{-1} (as in [11]), the previous results were quantitatively reproduced. To investigate the situation for other Raman modes, two other linewidths were also considered, one of 100 cm^{-1} corresponding to the effective resonance width of C-H stretch of lipid droplets in cells and one of 400 cm^{-1} corresponding to the linewidth of the O-H stretch in water. The nonresonant $\chi^{(3)}$ signal was set to be four times larger than the peak of the resonant signal. The intensities from the resonant and nonresonant contributions to $\chi^{(3)}$ were calculated separately. In Fig. 1(a) calculated resonant and nonresonant signals are shown as a function of pulse duration for different Raman resonances. As expected, using pulses of spectral width much larger than the Raman linewidth of interest leads to almost no gain in resonant signal (I_r), whereas the nonresonant signal (I_{nr}) only continues to increase, leading to poorer contrast. While not shown here but in agreement with previous work, the contrast continuously increases as the spectral pulse width decreases. However, the increase in contrast is at the expense of the magnitude of the resonant signal. Having high contrast but poor signals is of little value to users. Conversely, having large signals but poor contrast is also of little value. To this end, we define a parameter, the performance \mathbb{P}_f , which takes into account both contrast and signal levels. We define \mathbb{P}_f to be the contrast (I_r/I_{nr}) multiplied by the resonant signal I_r . This is plotted in Fig. 1(b) where it is clear, as intuitively expected, that optimal performance \mathbb{P}_f is achieved when the excitation pulse spectral width is equal to the Raman linewidth of interest. In particular, for lipids, the spectral linewidth should be 100 cm^{-1} , corresponding to a TL temporal pulse width of 173 fs FWHM, and for water the spectral width of the pulse should be 400 cm^{-1} , corresponding to a TL pulse of 43 fs FWHM. Note that the spectral resolution of the CARS process is given by $(\Delta_p^2 + \Delta_s^2)^{0.5}$ which implies that optimal performance is achieved when the spectral resolution is larger than the linewidth of interest.

Inspection of Fig. 1(a) suggests the nonresonant signal would overwhelm the resonant signal in almost all cases. The values used for the relative strength of the resonant and nonresonant $\chi^{(3)}$ and Raman linewidth in [11] are empirical values based on CARS measurements (calculated using the method of [18]). In order to determine those values for other Raman modes, explicit measurements of the contrast ratio in the microscope were performed, in our case for lipid imaging. This was done in two ways, as shown in Fig. 2. First, the total CARS signal was measured as the focus of the microscope objective was scanned from the glass coverslip (nonresonant signal only) to a drop of octadecene oil (strong resonant plus nonresonant signal). As seen in Fig. 2(a), the resonant signal from the oil is much larger than the nonresonant signal from the glass. To alleviate concern that this is due to a change in the nonresonant $\chi^{(3)}$ on going from glass to oil or a change in focussing conditions due to the change of medium, a

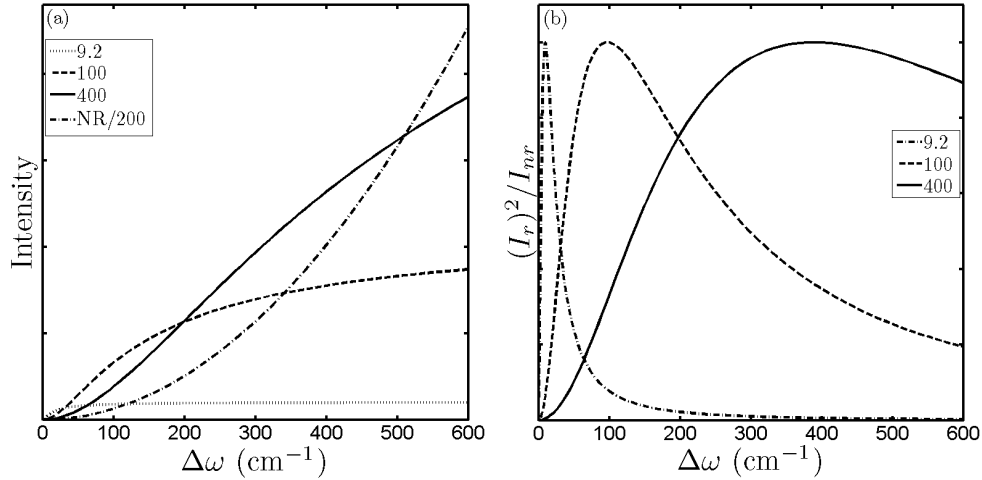


Fig. 1. (a) Theoretically predicted resonant and nonresonant CARS signal levels are plotted as a function of pump and Stokes spectral width. The three resonant curves correspond to the Raman linewidth of polystyrene beads 9.2 cm⁻¹, lipids 100 cm⁻¹ and water 400 cm⁻¹. The nonresonant signal (NR) is plotted for comparison. (b) The performance \mathbb{P}_f , the contrast ratio I_r/I_{nr} multiplied by the absolute signal level I_r , is shown as a function of pulse spectral width. It can be seen that \mathbb{P}_f peaks when the spectral width of the pump and Stokes matches the linewidth of the Raman mode being probed.

spectral scan of octadecene (using a method discussed below) was performed. As seen in Fig. 2(b), the ratio of resonant signal to nonresonant background is again very large and consistent with that implied by Fig. 2(a). Specifically, these measurements self consistently yield a contrast ratio of 40:1 when using 40 cm⁻¹ spectral width resolution. It is therefore likely that the calculations have overestimated the nonresonant signal in the lipid region by a significant amount. This seems consistent with observation of high quality CARS images in many laboratories. The above discussion suggests that we should consider optimizing the spectral pulse width when CARS imaging molecules having very different Raman linewidths.

It is in practice difficult to tune the TL laser spectral (or temporal) width of a given laser oscillator over a large range (e.g. 50 fs to 5 ps). This is even more challenging for the case of CARS where it would be necessary to simultaneously tune the spectral widths of two independently tuneable lasers, without introducing any relative timing or pointing changes. However, this problem can be readily overcome by spectral focussing of chirped pulses. We elaborate this point by considering resonant CARS signals, using the same model for the electric fields as above but now introducing linear chirp. We examine the first two steps of the CARS process since the CARS resonance is at second order. The pump-Stokes interaction for unchirped pulses is given by:

$$E_p(t)E_s^*(t) = E_p E_s \sqrt{\frac{\pi^2 \Delta_p \Delta_s}{(2 \ln 2)^2}} \exp\left(\frac{-\pi^2 (\Delta_p^2 + \Delta_s^2) t^2}{2 \ln 2}\right) \exp(i(\omega_p - \omega_s)t) \quad (1)$$

where E_j , Δ_j and ω_j (j given by p for the pump, s for the Stokes) are the magnitude, spectral width and center frequency of the respective pulses. In the case of chirped pulses, the pump-Stokes interaction is given by:

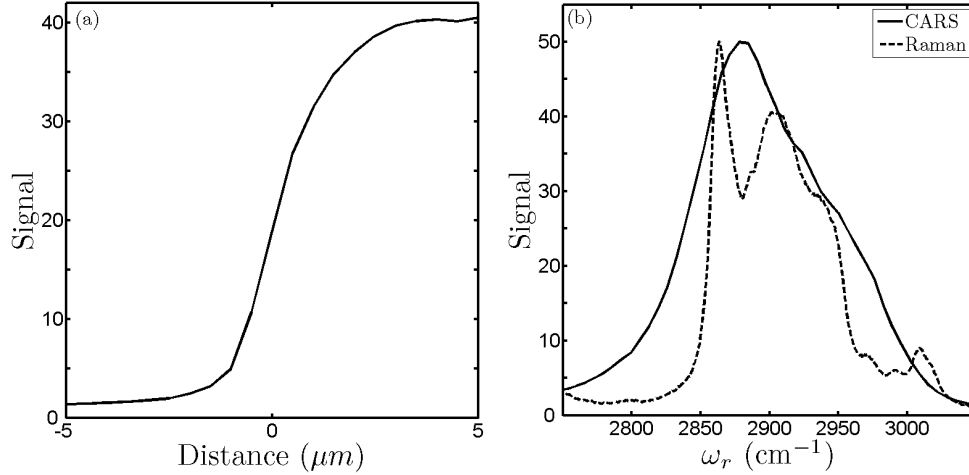


Fig. 2. Determination of resonant versus nonresonant CARS signals in the lipid region (effective pulse spectral widths of the pump and Stokes were $\sim 40 \text{ cm}^{-1}$). (a) The intensity profile of the laser focus was scanned along the axial direction across an interface from glass (purely nonresonant CARS signal) to octadecene (resonant CARS signal). The resonant signal was much larger. (b) A spectral scan of octadecene showing the line shape and the contrast between on and off resonant signal levels. For comparison, the spontaneous Raman spectrum of octadecene is included. These two scans yield a ratio of resonant to nonresonant signal exceeding 40:1, indicating that the resonant signal was not overwhelmed by the nonresonant background.

$$\begin{aligned}
 E_p(t)E_s^*(t) &= E_p E_s \sqrt{\frac{\pi^2 \Delta_p \Delta_s}{(2 \ln 2 + ia)(2 \ln 2 - ib)}} \\
 &\exp \left[-\pi^2 2 \ln 2 t^2 \left(\frac{\Delta_p^2}{(2 \ln 2)^2 + a^2} + \frac{\Delta_s^2}{(2 \ln 2)^2 + b^2} \right) \right] \\
 &\exp \left[i(\omega_p - \omega_s)t + i\pi^2 t^2 \left(\frac{\Delta_p^2 a}{(2 \ln 2)^2 + a^2} - \frac{\Delta_s^2 b}{(2 \ln 2)^2 + b^2} \right) \right] \quad (2)
 \end{aligned}$$

where a and b are the chirp parameter of the pump and Stokes pulses respectively. If we assume that the pump and Stokes pulses have the same spectral bandwidth ($\Delta_p = \Delta_s$) and chirp parameter ($a = b$), the chirped pulse expression simplifies considerably:

$$E_p(t)E_s^*(t) = E_p E_s \sqrt{\frac{\pi^2 \Delta^2}{(2 \ln 2)^2 + a^2}} \exp \left(\frac{-\pi^2 4 \ln 2 \Delta^2 t^2}{(2 \ln 2)^2 + a^2} \right) \exp(i(\omega_p - \omega_s)t) \quad (3)$$

Comparing the chirped with the unchirped case, we find that the former is mathematically identical to the case of a much narrower effective spectral width. This effective width is given by:

$$\Delta_{\text{effective}} = \sqrt{\frac{\Delta^2}{1 + \left(\frac{a}{2 \ln 2}\right)^2}} \quad (4)$$

For the CARS process at second order, this means that chirping large spectral bandwidth (fs) pulses is equivalent to using longer duration (ps) TL pulses of the same pulse energy. As the maximal spectral width is limited by the laser source itself, fs laser pulses (having large spectral bandwidths) provide a flexible CARS laser source since, with sufficient chirp, they can be made to behave like any pulse (fs to ps) having a narrower spectral width.

3. Materials and methods

A depiction of the optical arrangement is given in Fig. 3. A Spectra Physics Tsunami Ti:Sapphire laser system produced pulses of 60 fs at 80 MHz with 550 mW total average power. In most cases the laser was operated at a center wavelength of 800 nm. A Faraday isolator was used to avoid back reflections into the laser. The pulse train was sent through a prism compressor optimized for shortest pulse duration at the input to the PCF. The Ti:Sa beam was split by a 50:50 beam splitter into a pump and Stokes arm. The pump proceeded to the sample via a variable time delay stage and its average power was controlled by a variable neutral-density filter. The remaining 250 mW of power was directed to a PCF (NL-1.4.775-945, Crystal Fiber) which was previously shown to generate pulses in the near infrared [19]. The fiber also generated light in the visible which was filtered before the Stokes and pump were recombined. Typical powers before the microscope scan head were 12 mW in the Stokes and, depending on the sample, 40 to 150 mW in the pump. To control the chirp in the simplest possible way, we used fixed length blocks of glass: one 3 cm block of SF6 glass was placed in the pump arm and a 5 cm block of SF6 glass was placed in the Stokes arm to achieve nearly matched chirps. It is straight forward to implement an optical scheme wherein the degree of pulse chirp is continuously variable, such as by making use of prism or grating based zero dispersion line. This should permit continuous tuning of the effective CARS spectral resolution from $\sim 5 - 400 \text{ cm}^{-1}$. The power in the Stokes arm dropped to about 7 mW with the glass in place while the power in the pump remained unchanged (the glass blocks were AR coated for 800 nm). Note that these powers were attenuated by about a factor of ~ 2 through the microscope system before reaching the back aperture of the objective.

All imaging was performed on a modified Olympus Fluoview 300 (FV300) laser scanning system and IX71 inverted microscope. A 40X 1.15 NA UAPO water immersion lens with a cover slip correction collar was used as the objective and a 0.55 NA long working distance condenser lens for collection in the forward direction. The efficiency of collection in this configuration was insensitive to small adjustments of the focus of the collecting lens. Fluorescence signal was collected through the objective lens (epi-detection). A 400 - 700 nm filter (E700sp, Chroma Technology Vermont USA) was used to discriminate TPF, SHG, sum frequency generation (SFG) and anti-Stokes signals from the pump and Stokes beams. To discriminate forward propagating second-harmonic and CARS signals, additional band-pass filters were used. For imaging, light was directed to photomultiplier tubes (PMT) with enhanced red sensitivity (Hamamatsu R3896).

For myelin imaging, freshly excised rat dorsal root nerves were fixed in isotonic buffer containing 4% paraformaldehyde. The axon fibers were imaged while immersed in isotonic buffer between two cover slips using cut pieces of cover-slips as spacers (approximately 0.17 mm thickness). For multimodal imaging, aorta sections from 6 month old WHHLMI (Watanabe heritable hyperlipidemic myocardial infarction) rabbit strain [20] were prepared by fixing in 4% paraformaldehyde in phosphate buffered saline. Human Hepatoma cell line HuH-7 was grown in Dulbecco's modified Eagles medium (DMEM) supplemented with 100 nM nonessential amino acids, 50U/ml penicillin 50 $\mu\text{g/ml}$ streptomycin and 10 percent fetal bovine serum. Methanol used as test samples was reagent grade.

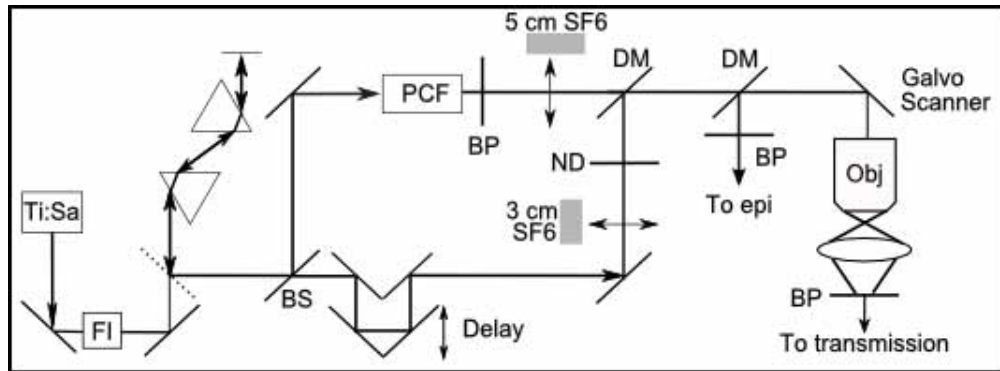


Fig. 3. Multimodal CARS microscopy optical arrangement. Pulses from the Ti:Sa oscillator are sent through a Faraday isolator (FI) followed by a prism compressor. A 50:50 beam splitter (BS) divided the incoming light. One arm was sent through a photonic crystal fiber (PCF) and bandpass filter (BP) before being recombined on a dichroic mirror (DM). The other half was sent through a time delay arm that included a neutral density filter (ND). In both the pump and Stokes paths, glass (SF6) could be added to control the chirp. The recombined beam was sent into the FV300 microscope. Inside the FV300, there were more dichroic mirrors and filters to separate the signals from the excitation light. Note that the epi-detected fluorescence signals were collected inside the microscope.

4. Results

In practice, the spectral pulse width of the pump and Stokes are not identical as was assumed in the discussion of the theory of chirped pulse CARS above. In our case, the Stokes spectrum from the PCF is much broader than the pump spectrum. The unused Stokes spectrum does not contribute to CARS signal generation, nor does it negatively impact cell viability: the Stokes power is significantly lower than the pump and is further to the infrared where absorption is significantly lower. In fact, the broad spectrum of the Stokes can be used to our advantage. Since the pulses are chirped, changing the time delay between the pump and Stokes pulses changes the instantaneous difference frequency and therefore the Raman mode being probed. This is illustrated in Fig. 4 where the instantaneous frequency of the pulses is plotted as a function of time. In Fig. 4(a) we show the case where the pump and Stokes pulses have unmatched chirp, resulting in poor spectral resolution $\Delta\Omega$. In Fig. 4(b) we show the case where the pulses have matched chirp. Here the frequency difference between the pulses is constant giving enhanced spectral resolution $\Delta\Omega$. Changing the time delay between the pulses changes frequency difference and thus the Raman mode probed Ω_1 , Ω_2 . This gives a simple rapid method of scanning across the Raman modes of the sample.

Using different chirp conditions (no glass, or 3 cm SF6 in the pump arm and 5 cm SF6 in the Stokes arm giving nearly matched chirp), CARS spectra of liquid methanol were taken using the FV300, the results being shown in Fig. 5. In the case of no glass, there is still some residual, yet unmatched chirp, due to the microscope internal optics and the objective. As can be seen by comparing the methanol spectra, increasing the pulse chirp improves spectral resolution. When the pump and Stokes are chirped, the two peaks of methanol around 2835 and 2944 cm^{-1} [21] are better resolved and can be clearly distinguished. The FWHM of the methanol 2835 cm^{-1} band is $\sim 25 \text{ cm}^{-1}$ [22], allowing a crude estimate of the spectral resolution. With the two blocks of glass in place, the measured FWHM of the band is $\sim 65 \text{ cm}^{-1}$ indicating a spectral resolution of 60 cm^{-1} . When the pulses were chirped using the blocks of glass, the CARS signal levels dropped slightly, but not as quickly as did the SHG and TPF signals. This

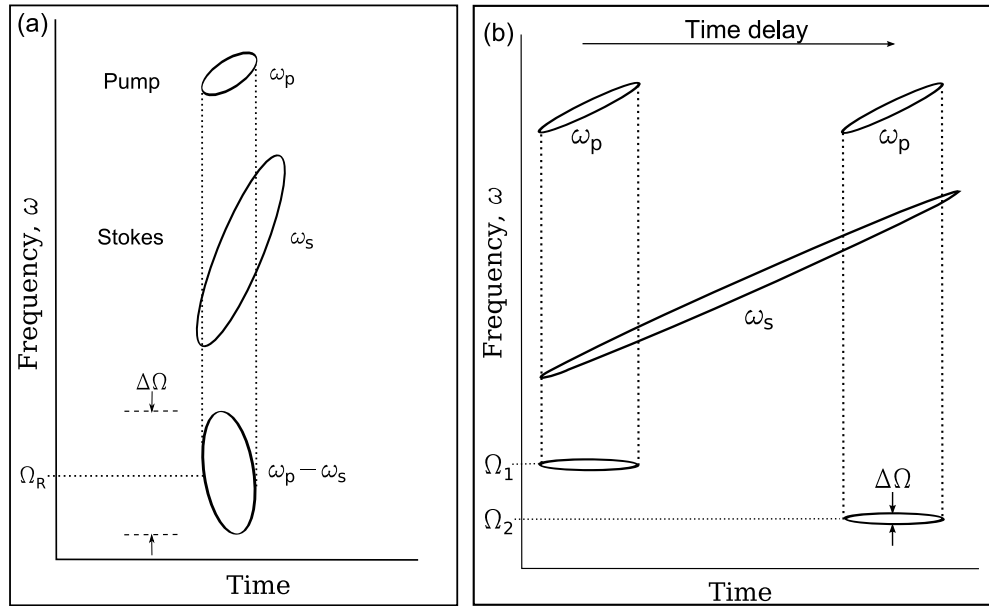


Fig. 4. Time-frequency plots showing the pump and Stokes pulses as ellipses in (ω, t) space. In this representation, transform limited pulses have vertical major axes whereas those of chirped pulses are tilted. The instantaneous bandwidth is determined by measuring the height of an ellipse at any instant of time. In CARS, the spectral resolution is set by the first two photon interactions and, in this representation, the spectral resolution $\Delta\Omega$ is determined by the total height of the ellipse $\omega_p - \omega_s$. (a) Pulses having unmatched chirps and large instantaneous bandwidths. Here, the spectral resolution $\Delta\Omega$ is poor because the instantaneous bandwidth is large and the difference between the pump and Stokes is changing as a function of time. (b) Chirp matched pulses with narrow instantaneous bandwidths. Here the spectral resolution $\Delta\Omega$ is improved because the instantaneous bandwidths of both the pump and Stokes are narrower and the frequency difference between the pump and Stokes is nearly constant. It is seen that changing the time delay between pump and Stokes scans the instantaneous difference frequency, corresponding to different Raman modes being probed (Ω_1, Ω_2).

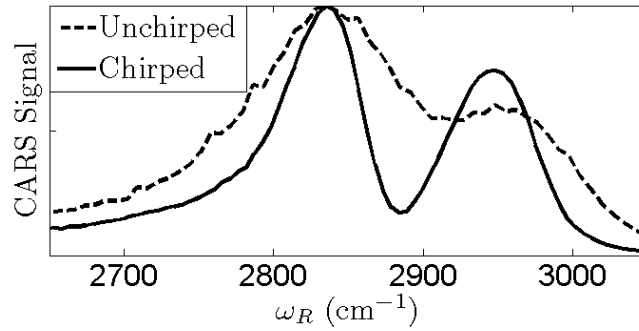


Fig. 5. FV300 CARS spectrum of methanol obtained by scanning the time delay between the pump and Stokes pulses. One curve (dashed) was obtained with near transform limited pulses having large instantaneous bandwidths and unmatched chirps (corresponding to Fig. 4(a)). The second curve (solid) was obtained with pulses that were nearly chirp matched and narrow instantaneous bandwidths (corresponding to Fig. 4(b)). As expected, varying the chirp and ensuring matched chirp rates improves the spectral resolution. In this case, the spectral resolution varied from $>160 \text{ cm}^{-1}$ to $<60 \text{ cm}^{-1}$.

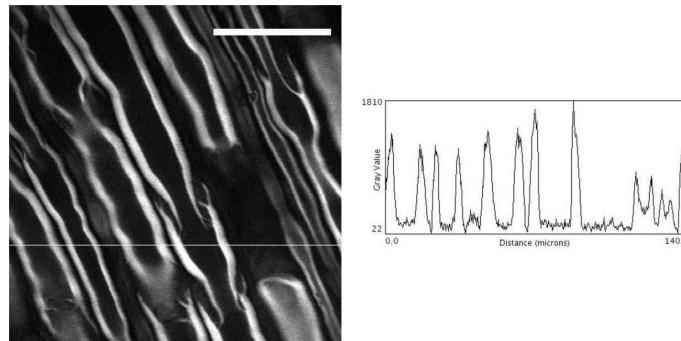


Fig. 6. Forward detected FV300 CARS imaging of fixed rat dorsal root nerves. The CARS resonance was set to 2850 cm^{-1} . The lipid-rich myelin sheath surrounds the neuronal axon and generates a strong CARS signal. The pixel intensity profile of the indicated line is shown, revealing high contrast. The scale bar is $50 \mu\text{m}$. The pixel dwell time was $8 \mu\text{s}$.

is expected since the resonant CARS signal should only drop significantly when the effective pulse spectral width is less than the Raman linewidth (see Fig. 1(a), whereas SHG and TPF signals fall as the intensity is reduced).

In Fig. 6 we show measurements of rat spinal nerves, demonstrating the capability of using this system for CARS tissue imaging. The spinal nerves are approximately $300 \mu\text{m}$ in diameter and consist of bundles of roughly 100 myelinated axons, each about $15 \mu\text{m}$ diameter. The effective depth of field of the CARS signal was $\sim 1.5 \mu\text{m}$, necessary in order to see details in this tissue. The pixel intensity profile of the indicated line is shown, demonstrating the contrast achieved. It is clear that the signal intensity from the myelin is at least 60 fold greater than that from the axon and that fine detail in the myelin structure is clearly visible. In work not presented here, the spectral response of the myelin was measured, clearly demonstrating that the signals observed were solely due to Raman resonant enhancement, rather than changes in the nonresonant $\chi^{(3)}$.

In Fig. 7 we show an atherosclerotic lesion from a rabbit aorta which was used as a test

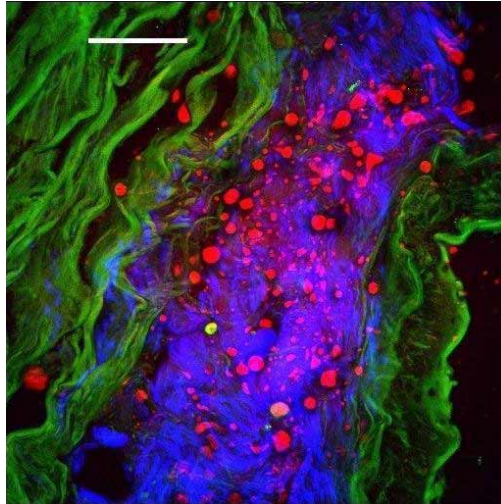


Fig. 7. Multimodal CARS microscopy of rabbit aorta. A 50 micron thick section of aorta was tangentially cut to the luminal side and imaged for lipids (CARS - red) collagen (second harmonic - blue) and smooth muscle elastin (fluorescence - green). All three signals are endogenous to the sample. The CARS and SHG were collected in the forward direction whereas the TPF was collected in the epi-direction. This image is a z-projection of a 50 image data set of a 3D scan through the sample (images set $1 \mu\text{m}$ apart). The scale bar is $50 \mu\text{m}$. The pixel dwell time was $8 \mu\text{s}$.

sample for label free multimodal imaging. A $50 \mu\text{m}$ section of aorta tangential cut to the luminal side was imaged showing lipids (CARS - red), collagen (SHG - blue) and smooth muscle elastin (TPF - green). It should be noted that all three signals are endogenous to the sample and no dyes or stains were added to enhance contrast. These images were taken without the additional SF6 glass in place because high spectral resolution was not required, while the higher intensity allowed deeper penetration into the tissue (for pulses of constant energy, maximum intensity allows maximum depth penetration). The image is a projection of a 50 image data set recorded along the axial direction ($1 \mu\text{m}$ interval between images). An extensive network of collagen surrounds the lipid rich tissues, suggesting a stage V or later, type lesion [23].

5. Discussion

For high performance imaging (512×512 pixels), a CARS laser system must be stable on a broad range of time scales. For our modified FV300, pixel dwell time ranged from 2-50 μs . Line scanning time scales were from 1-25 ms, while the acquisition of a whole image ranged from 1-30 s. We find that the laser source described here is stable on all these time scales. This system is therefore quite useful for imaging live cells and tissue for samples which are adversely affected by irradiation: any laser source requiring increased pixel dwell time and/or frame averaging to overcome source noise cannot be considered practical. It should be noted that while most imaging work in this paper used a pixel dwell time of $8 \mu\text{s}$, we routinely used 2 μs for alignment and for the imaging of live cells. To test long term stability, we acquired a one hour long time-course movie of live human liver cells (HuH 7 cells), with images taken every fifteen seconds. Images from the beginning and end of the time course can be seen in Fig. 8 and the entire video is available online as supplementary material. The video demonstrates that our CARS laser source is stable on all time scales relevant to live cell microscopy.

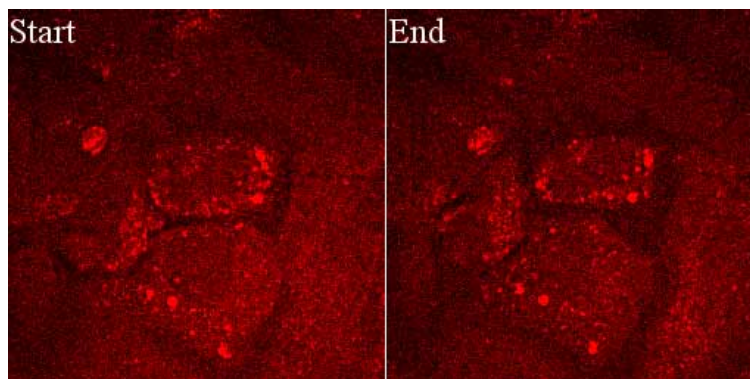


Fig. 8. (Media 1) CARS video of lipid trafficking in live human liver cells. Here we show the first and last frames from a hour long time course of live HuH 7 cells, using label-free CARS imaging of lipids. The full video is available online. The high stability of this multimodal CARS microscope allows near continuous imaging of live cells.

Having a constant frequency difference between the pump and Stokes pulses at the sample permits the mapping of CARS resonances onto the position of a delay stage that controls the time delay of the pump relative to the Stokes pulse. Our system permits tuning of the resonant Raman frequency from 2500 cm^{-1} to 4100 cm^{-1} , with 60 cm^{-1} (or better) spectral resolution. This includes the regions of the C-H stretch of lipids and the O-H stretch of water. Note that the PCF is capable of producing similar output when pumped with longer wavelengths, so that the C-D Raman mode at $\sim 2100\text{ cm}^{-1}$ or even the fingerprint region below 1600 cm^{-1} should be accessible by tuning the Ti:sapphire oscillator to 900 nm [24]. Conveniently, these spectral regions (O-H, C-H, C-D, and the top of the fingerprint region) are well separated from each other, making it feasible to tune amongst these bands.

When imaging deep in tissue samples, the increased scattering and absorption losses incurred by all signals leads to a case where the use of shorter pulses to increase signal from SHG and TPF is more important than the reduction of CARS spectral resolution. The ability to routinely balance the CARS resolution versus signal from other nonlinear optical processes for a given sample is only available when using chirped fs pulses. Given the significantly increased versatility of fs pulses, it is likely that fs sources will be used with increasing frequency for CARS microscopy. While the PCF based setup offers a simple, single laser source for CARS microscopy, the ideas presented here on optimal performance and use of pulse chirp are applicable to any fs system. Relevant examples include the use of two synchronized fs lasers or fs OPOs. Either of these sources could equally benefit from the use of tunable pulse chirp to achieve optimal performance.

6. Conclusion

We have presented a spectral focussing implementation of live cell CARS microscopy wherein the degree of linear chirp is considered an active variable. The best compromise between contrast and absolute signal levels for CARS microscopy is achieved when the effective pump and Stokes pulses spectral widths matches the Raman linewidth of interest. This condition can be achieved by using chirped fs pulses with careful control over the pulse chirp. By using chirp as a control parameter, the microscope user can choose to optimize contrast in CARS imaging or enhance signals in various nonlinear optical processes (e.g. CARS, TPF, SHG, THG, etc.) in a multimodal microscope. Finally, as shown here, we note that if one of the pulses has a much

broader spectrum than the other, it is possible to perform rapid multiplex CARS imaging by simply scanning the time delay between the pump and Stokes, obviating the need to tune any lasers. The images and video presented here demonstrate that this approach leads to a practical, yet high performance multimodal CARS microscope.

Acknowledgments

The assistance of Jennifer Haley and Rodney Lyn for the HuH-7 cells, Ileana Micu at the Ottawa Health Research Institute for rat dorsal root nerves, and Michael Sowa and Alex Ko at Institute for Biodiagnostics, National Research Council of Canada, Winnipeg, Manitoba Canada for rabbit artery samples are gratefully acknowledged. We thank the Canadian Institute of Health Research (CIHR) Regenerative Medicine and Nanomedicine team grant #RMF79032 for financial support. A.P. would like to thank NSERC, Alberta Scholarship Program, and NRC for funding support. Department of Physics, Queen's University, Kingston, ON, K7L 3N6